Sandstone landforms shaped by negative feedback between stress and erosion

Jiri Bruthans[1], Jan Soukup[1], Jana Vaculikova[1], Michal Filippi[2], Jana Schweigstillova[3], Alan L. Mayo[4], David Masin[1], Gunther Kletetschka[1], Jan Rihosek[1]

[1]Faculty of Science, Charles University in Prague, Albertov 6, 128 43 Prague 2, Czech Republic. [2]Institute of Geology, AS CR, v. v. i., Rozvojova 269, 165 00 Prague 6, Czech Republic. [3]Institute of Rock Structure and Mechanics, AS CR, v. v. i., V Holesovickach 41, 182 09 Prague 8, Czech Republic. [4]Brigham Young University, Department of Geosciences, Provo UT 84602, USA.

First paragraph (199 words)

Weathering and erosion of sandstone produces spectacular enigmatic[1,2] landforms such as arches, alcoves, pedestal rocks and pillars. Despite of multiple diverse ideas about their origin, no experiments produced realistic landforms[1,2]. The effect of gravity loading stress has been overlooked[3] or assumed to increase the landform's weathering rate[4,5]. Here we show by physical and numerical modelling, and field observations of locked sands and sandstones that an increase in stress within the landform reduces weathering and erosion. Material with insufficient loading is rapidly removed by weathering process and the remaining load bearing landform structure is protected by the fabric interlocking mechanism. As the landform evolves the increased stress inhibits erosion from raindrop impact, flowing water and slaking, and retards surface retreat caused by salt and frost weathering. Planar discontinuities in sandstone and negative feedback between stress and weathering/erosion processes are sufficient conditions to create landforms. We interpreted this by a novel mechanical model and verified in laboratory where we created arches, alcoves, pedestal rocks and pillars using landform material and mimicking natural processes. We supported the proposed negative feedback mechanism by a numerical model of stress pattern in landforms. Our findings show that this mechanism coordinates weathering/erosion while carving sandstone landforms.

Text (1797 words)

Factors considered in the origin of sandstone landforms include quartz dissolution[1], salt and frost weathering[6], sapping[7], thermal expansion[8], biogenic activity[9], incipient fractures[10], exfoliation[1], case hardening[11], moisture flux[12] and diffusion[13]. Prior experimental investigations have focused on salt and frost weathering[14,15,16]. Planimetric curvature of sandstone amphitheatres have been explained by the interlocking of joined blocks[1,17], and the evolution of arches and bridges have been explained by fracture propagation[1,18,19]. The destructive effect of stress generated by overburden loading has been considered in the evolution of towers and cliffs[5]. Several groups have shown that small forms may be linked morphologically to stress[13,20], but these authors did not explain the mechanisms involved. Their work did not describe what stabilizes the upper surface of arches and other similar landforms so they can remain freestanding in an otherwise denudated surface (Fig. 1a).

Granular sediment may behave as a strong, rock-like material due to the following mechanisms which stabilise sediment fabric[21]: 1) Capillary cohesion from interfacial-tension caused by partial water saturation[22]; 2) Electrochemical cohesion by van der Walls forces acting between clays particles[21]; 3) Cementation cohesion from grain-to-grain cementation and; 4) Fabric interlocking of subangular grains[21,23]. Fabric interlocking is caused by preferential dissolution of stressed material at grain contacts and its re-precipitation in voids, causing increase of the grain contact area and decrease of sediment porosity. Capillary cohesion is lost and electrochemical cohesion in clay bridges is reduced when a sandstone becomes fully saturated[24,25]. When sandstone's surface weathers, the cementation cohesion degrades, leaving fabric interlocking as a primary factor inhibiting surface disintegration. Here we report: 1) The first laboratory experiments that show a general mechanical behaviour of fabric interlocked material exposed to specific weathering/erosion processes under various stress levels (irrespective of the shape of the landform); 2) Interpretation of the results by a novel material model; 3) Previously unreported effects of salt and frost weathering of cemented sandstones under controlled stress and; 4) The first physical and numerical modelling of selected small-scale landforms with specific boundary conditions. The origin of sandstone arches (bridges), alcoves (rock shelters and overhangs), pedestal rocks (mushroom shaped pillars) and cavity/pillars are of special interest in this paper.

Oven dried cubes of sandstone from Strelec Quarry (SLS, Methods) are stable in the absence of an external load due to electrochemical cohesion in clay bridges (Supplementary Figure 7), however the same SLS cubes quickly disintegrate when immersed in water. We attribute this disintegration to the decrease of the electrochemical cohesion accompanied by surface slaking. This occurs as entrapped air in the pore space is compressed by surface tension forces due to entering water, which exerts sufficient pressure on pore sides to compromise the stability of the material fabric (see Supplementary Information). However, when a cube of SLS is subjected to sufficient vertical stress and immersed in water, the disintegration of the vertical sides proceeds until a stable shape evolves (Fig. 2a). Initially the vertical stress in the landform is relatively small due to the large area distribution of the vertical load. The "hour glass" shape thinning of the original cube reduces the cross-sectional area of the forming structure (Fig. 2a), thus increasing the stress. When the stress reaches a critical value (critical stress) it triggers the stabilization of the locked fabric which defines the final shape which is resistant to further erosion. The nature of the fabric-locking due to the stress field is illustrated in the following experiment. We loaded SLS cubes with an initial vertical force of 10 N and immersed the loaded cubes in water to obtain the initial stabilization form. Subsequently, we decreased the applied force in steps and measured the area Ssat after each stabilization event (step) with respect to the calculated critical stress (Fig 2b). Critical stress remained relatively constant (0.5-2.6 kPa) until the Ssat decreased below 20% of its original size (<0.002 m^2).

The critical stress then increased rapidly (up to 8 kPa, Fig. 2b) and the surface of elliptical pillars progressively altered into rib texture and lines that paralleled the principal stress directions (Fig. 2a). Similar features can be observed on surfaces of natural landforms (Supplementary Fig. 8).

In the second experimental set we measured saturated tensile strength on 50 cubes of SLS (Fig. 2c). Cubes of ten cm in size were uniaxially loaded (Methods). The mean tensile strength of unconfined water saturated SLS cubes under reduced atmospheric pressure of 2 kPa was measured less than 0.5 kPa (Fig. 2c). When the cubes were axially loaded (uniaxial load 250-1500 kPa; Fig. 2c) the measured mean saturated tensile strength was 4 kPa. In addition to the above experiments, we studied the global strength of the fabric locked material in uniaxial compression and axisymmetric compression with constant radial stress. Although the unconfined specimens easily disintegrated into individual grains, the loaded material showed considerable uniaxial strength (3 MPa) and a high angle of internal friction (72°) (Supplementary Information). High strength in locked sands have also been observed previously by different authors[26,27,28].

We propose the following continuum mechanical interpretation of the behavior of locked sands. Brittle material failure can be described by the standard failure envelope of plasticity theory (Fig. 3). It is characterized by a high friction angle of 72° and non-negligible tensile strength of 1 to 10 kPa. However, for low stress levels we discovered a conceptually new behaviour. In this case the material does not fail in a brittle and highly dilatant manner, as typical for sheared fabric-locked materials, but instead the fabric degrades completely and the material disintegrates into individual grains. To describe this observation, we propose a stress region denoted as "*locus of fabric instability*" (Fig. 3). The fabric disintegrates once the complete Mohr circle falls within this locus. A tensile strength of ≤0.5 kPa, measured on saturated SLS without load, represents the lower stress boundary of the locus of fabric instability. The critical stress, where disintegration of the uniaxially loaded sample stops (approximately 1-8 kPa), represents the upper stress boundary. While the global strength envelope follows from the conventional plasticity theory, the locus of fabric instability or its equivalent has not yet been described. Unlike the global envelope, the locus of fabric instability is not a pure material property, but it reflects the actual disintegration process (an increase of disintegration process energy increases the size of the locus of fabric instability). The concept of locus of fabric instability explains in a rational manner negative feedback between stress and erosion.

We also investigated different erosion processes. To investigate the effect of surface slaking, we repeated prior disintegration tests on unconfined samples inside a desiccator under reduced air pressure (2 kPa). The samples preserved their shape under reduced pressure and stayed stable. However, the same samples spontaneously disintegrated when dried and immersed again in atmospheric pressure. This observation indicates that surface slaking is the leading disintegration process in our experiments. To further investigate the erosion processes we exposed SLS cubes to simulated rain and flowing water (Methods). Unconfined cubes completely eroded away by simulated rain within 5-7 minutes with one exception (Supplementary Table 8), whereas uniaxially loaded cubes attained a stable geometry and erosion ceased after ~60 minutes leaving ~70% of the cube volume intact. Similarly, none of the uniaxially loaded SLS cubes were eroded by fast flowing water (~10 cm /s), whereas unconfined cubes were eroded in few tens of seconds. Another possible source of weathering is due to salt and frost. We used several cemented sandstones from the Czech Rep. and USA to evaluate how this disintegration responds to the level of uniaxial load (Methods).

Unconfined cubes of cemented sandstones, subjected to salt and frost weathering, disintegrated up to 4 times faster than the uniaxially loaded cubes. Such uniaxially loaded cubes weathered to thin “hour glass” columns, resembling landforms found in nature (Fig. 2d; Supplementary Figs. 10, 11; Supplementary Table 9).

In the principal part of our study, we investigated development of sandstone landforms by means of physical modelling. We vertically loaded SLS blocks and partially immersed them in water. The portion of the block above the water level remained stable due to additional cohesion sources (such as capillary cohesion). The portion below the water level disintegrated into individual grains. This disintegration progressed until a stable landform evolved. An implication of the negative feedback between stress and erosion is that material that is not part of the load bearing structure, specifically the volumes where the stress does not exceed critical value, is rapidly removed by erosion while the load-bearing portion is protected during each period of landform evolution. This mechanism explains why the surfaces of natural arches, alcoves, pedestal rocks and pillars are relatively smooth, without significant protrusions. Stress in small protrusions is sub-critical, making protrusion prone to erosion. In our physical models, we were able to reproduce natural shapes such as arches, alcoves, pedestal rocks, and multiple pillars (Fig. 1). A subhorizontal discontinuity in the middle of a SLS block was the only necessary condition for arch formation. Alcoves were created when subhorizontal discontinuities partly undercut the SLS block. Undisturbed SLS blocks were transformed by surface disintegration into pedestal rocks or single pillars. Multiple discontinuities in SLS blocks led to the development of multiple pillars (Fig. 1, Supplementary Figs. 12- 17).

To visualise the stress field within the landforms we performed numerical modelling (finite element method). We modelled planar discontinuities, which led to development of arches and cave pillars in physical models. The principal stresses aligned around the discontinuity and formed the zone of low stress susceptible to erosion (Fig. 4).Importantly, modelling shows that the stress is higher at the upper parts of blocks directly above the discontinuities (Supplementary Fig. 18) and the modelling thus suggests that in this area stress protects most efficiently the surface of the developing arch from erosion. This provides an explanation why arches are often free standing. Furthermore, the models suggest that stress in protrusions sticking out from sandstone landforms is much lower than stress within the load-bearing structure. The stress in protrusions may fall within the locus of fabric instability, which leaves such shapes unprotected from weathering/erosion processes.

In this paper we have shown by experimental evidence using natural materials that retreat of some landforms due to erosion is stress field regulated. Low stress allows the disintegration of the material into individual grains, whereas high stress activates fabric interlocking and the material resists erosion. The global failure envelope and the locus of fabric instability allow a straightforward explanation of this erosion resistance. By means of unique physical modelling, we have developed analogues of natural sandstone arches, alcoves, pedestal rocks and pillars. We thus demonstrate that the stress field is the primary cause of the shape evolution of these landforms. In addition to the dominant role in origin of the above listed landforms, stress fields likely affect the weathering of many sandstone exposures including cultural heritage sites.

Methods (763 words)

Materials

Two types of sediments were used in the study: i) Locked sand from Strelec Quarry (Czech Republic) with no cementation cohesion and dominated by fabric interlocking (referred to as SLS) and ii) Sandstone and other sediments with dominant cementation cohesion (i.e cemented sandstones). The SLS from the quarry is so weak that it can be eroded by running water and rain and was mined for decades by spraying a jet of pressurized water[29]. The same material is mined by explosives when dry and prior to recent safety regulations SLS provided stable (up to 40 m high) vertical mining faces. Samples of SLS were cut from the many sandstone blocks by hand saw. For more information on sample selection and additional characterization of the SLS material, see Supplementary Information 2. For material behaviour measurements we used SLS material that was cut by hand saw into specimens of various sizes (see below). For physical modelling, rectangular blocks with sides up to 300 mm long and cylinders 100-150 mm in diameter were used. Samples of cemented sandstone represent different lithological and tectonic settings. They were collected from the Colorado Plateau (USA), and the Bohemian Cretaceous Basin (Czech Rep.), (Supplementary Table 3). Samples of cemented sandstones were cut by diamond saw cooled by water onto the cubes with edge lengths of 40±1 mm.

Measurement of sandstone mechanical behaviour

In the first set of experiments we studied conventional mechanical behaviour at high stress levels. Compression tests at constant radial stresses were performed in the VJT TriScan100 triaxial apparatus using 74 mm (length) by 38 mm (diameter) cylinders. The uniaxial compression tests were performed on 50 mm sandstone cubes in a load frame. The tensile strength of sandstone was measured on uniaxially loaded 100 mm sized cube specimens under controlled vertical load using a pull-of force by a tensiometer[29]. The vertical stress was imposed by placing the specimens into a steel frame and tightened by screws using torque screwdriver. Vertical load was calibrated by a tensiometer placed in the steel frame.

The second set of experiments studied fabric disintegration at low stress levels. The SLS specimens, stabilised by the natural state of partial saturation and by clay bridges between the particles, were cut into 100 mm sized cubes by gently hand sawing. When SLS cubes are completely immersed in water without axial load they quickly disintegrate. To measure the stress limit of fabric disintegration, the cubes were uniaxially loaded with an initial vertical force of 10 N applied by a lead weight. Initial form stabilization was achieved after immersion. The applied force was then decreased in steps and vertical stress within the sample was evaluated after form stabilization was achieved in each step. Tensile strength of unconfined specimens was measured using the same procedure as at uniaxially loaded specimens.

Erosion experiments on non-cemented and cemented sandstones

The disintegration mechanism due to surface slaking was investigated by reproducing the disintegration tests on unconfined samples in a desiccator at a reduced air pressure (2 kPa). To investigate the disintegration due to raindrop impact and flowing water, unconfined and confined SLS cubes were exposed to continuous artificial raindrop impact produced by a rain simulator. For this experiment we used the rainfall simulator Eijkelkamp version 09.06. Modelled rainfall had the following characteristics: Rain intensity = 6 mm/min, diameter of water droplets = 6 mm and rainfall's kinetic energy = 4 $J/m^2/mm$. Modelled rainfall was applied to pairs of SLS cubes. In each pair one cube was unconfined and the other was uniaxially compressed. To investigate the effect of salt and frost weathering, experiments for both unconfined and uniaxially loaded conditions were performed on three pairs of cubes from each sandstone type (Supplementary Fig. 5). Each cube was subjected to either salt or freezing weathering, in one day cycles, until complete disintegration occurred. Prior to each cycle, the cubes for the salt experiments were soaked in brine (Na_2SO_4) and the cubes for frost weathering were immersed in distilled water for eight hours prior to freezing.

Numerical modelling

Stress fields in sandstone landforms was visualised by finite element method using the software PLAXIS[30], version 2010. Sandstone was characterised using Mohr-Coulomb constitutive model with friction angle of 72°. Specimens were modelled at a laboratory scale. The stress field was imposed by gravity loading. The material model in the simulations did not include the locus of fabric instability. Instead, principal stresses were evaluated on simulation results and areas prone to fabric disintegration were identified based on the stress state.

For additional descriptions of the methods see Supplementary Information. Datasets from the article are available at http://dx.doi.org/10.6084/m9.figshare.1056303.

References

1. Young, R. W., Wray, R. A. L. & Young, A. R. M. *Sandstone Landforms* (Cambridge University Press, Cambridge, 2009).

2. Turkington, A. V. & Paradise, T. R. Sandstone weathering: a century of research and innovation. *Geomorphology* **67,** 229-253 (2005).

3. Viles, H.A. Scale issues in weathering studies. *Geomorphology* **41,** 63-72 (2001).

4. Gerber, E. & Scheidegger, A. E. Erosional and stress-induced landforms features on steep slopes. *Z. Geomorphol. Suppl.* **8,** 38-49 (1973).

5. Gerber, E. & Scheidegger, A. E. Stress-induced weathering of rock masses. *Eclogae Geol. Helv.* **62,** 401-415 (1969).

6. Williams, R. B. G. & Robinson, D. A. Weathering of sandstone by the combined action of frost and salt. *Earth Surf. Process. Landf.* **6,** 1-9 (1981).

7. Laity, J. E. & Malin, M. C. Sapping processes and the development of theater-headed valley networks on the Colorado Plateau. *Geol. Soc. Am. Bull.* **96,** 203-217 (1985).

8. Warke, P. A., McKinley, J. & Smith, B. J. Variable weathering response in sandstone: factors controlling decay sequences. *Earth Surf. Process. Landf.* **31,** 715-735 (2006).

9. Mustoe, G. E. Biogenic origin of coastal honeycomb weathering. *Earth Surf. Process. Landf.* **35,** 424-434 (2010).

10. Cruishank, K. M. & Aydin, A. Role of fracture location in arch formation, Arches National Park, Utah. *Geol. Soc. Am. Bull.* **106,** 879-891(1994).

11. Conca, J. L. & Rossman, G.R. Case hardening of sandstone. *Geology* **10,** 520-523 (1982).

12. Conca, J. L. & Astor, A. M. Capillary moisture flow and the origin of cavernous weathering in dolerites of Bull Pass, Antarctica. *Geology* **15,** 151–154 (1987).

13. McBride, E. F. & Picard, M. D. Origin of honeycombs and related weathering forms in Oligocene Macigno Sandstone, Tuscan coast near Livorno, Italy. *Earth Surf. Process. Landf.* **29,** 713-735 (2004).

14. Rodriguez-Navarro, C., Doehne, E. & Sebastian, E. How does sodium sulfate crystallize? Implications for the decay and testing of building materials. *Cem. Concr. Res.* **30,** 1527-1534 (2000).

15. Smith, B. J., Warke, P. A., McGreevy, J. P. & Kane, H. L. Salt-weathering simulations under hot desert conditions: agents of enlightenment or perpetuators of preconceptions? *Geomorphology* **67,** 211-227 (2005).

16. Ruedrich, J. & Siegesmund, S. Salt crystallisation in porous sandstone. *Environ. Geol.* **52,** 225-249 (2007).

17. Stacey, T. R. Technical note 2. The behaviour of two- and three- dimensional model rock slopes. *Q. J. Eng. Geol.* **8,** 67-72 (1974).

18. Stephansson, O. Stability of single openings in horizontally bedded rock. *Eng. Geol.* **5,** 5-71 (1971).

19. Robinson, E. R. Mechanical disintegration of the Navajo sandstone in Zion Cayon, Utah. *Geol. Soc. Am. Bull.* **81,** 2799–2806 (1970).

20. Mikuláš, R. Gravity and orientated pressure as factors controlling "honeycomb weathering" of the Cretaceous castellated sandstones (Northern Bohemia, Czech Republic). *Bull. Czech Geol. Surv*. **76,** 217-226 (2001).

21. Dusseault, M. B. Itacolumites: the flexible sandstones. *Q. J. Eng. Geol.* **13**, 119-128 (1980).

22. Hornbaker, D. J., Albert, R., Albert, I., Barabasi, A. L. & Shiffer, P. What keeps sandcastles standing? *Nature* **387,** 765 (1997).

23. Dusseault, M. B. & Morgenstern, N. R. Locked sands. *Q. J. Eng. Geol.* **12,** 117-131 (1979).

24. Dobereiner, L. & de Freitas, M. H. Geotechnical properties of weak sandstones. *Geotechnique* **36,** 79-94 (1986).

25. Lin, M. L., Jeng, F. S., Tsai, L. S. & Huang, T.H. Wetting weakening of tertiary sandstones-microscopic mechanism. *Environ. Geol.* **48,** 265-275 (2005).

26. Abdelaziz, T. S., Martin, C. D. & Chalaturnyk, R. J. Characterization of locked sand from Northeastern Alberta. *Geotech. Test. J.* **31,** 480-489 (2008).

27. Collins, B. D. & Sitar, N. Geotechnical properties of cemented sands in steep slopes. *J. Geotech. Geoenviron. Eng.* **135,** 1359-1366 (2009).

28. Cresswell, A. & Powrie, W. Triaxial tests on an unbonded locked sand. *Geotechnique* **54,** 107-115 (2004).

29. Bruthans, J. *et al.* Fast evolving conduits in clay-bonded sandstone: Characterization, erosion processes and significance for origin of sandstone landforms. *Geomorphology* **177-178,** 178-193 (2012).

30. PLAXIS Finite Element Code for Soil and Rock Analyses. PLAXIS-2D Version 8, Reference Manual, (eds Brinkgreve et al., DUT, the Netherlands, 2004). www.plaxis.nl

Correspondence and requests for materials should be addressed to J.B.

Acknowledgements: We acknowledge help of G. T. Carlig and D. Tingey for assistance with sampling and measurements in USA and J. Valek and J. Bohac for UCS and triaxial measurements. We also thank M. Audy, M. Sluka, V. Cilek and J. Adamovic for providing photographs and V. Erban, L. Palatinus, A.N. Palmer, K. Zak, J. Mls and T. Fischer for valuable comments on this manuscript. Rain simulator was provided by VUMOP, Prague. This research was funded by the Grant Agency of Charles University (GAUK No. 380511), Czech Science Foundation (GA CR No. 13-28040S), the research plan No. RVO 67958531 and MEYS grant LK21303. The research was also supported in part by the Hintze Fund at Brigham Young University, Provo, UT, USA.

Author Contributions: J.B. proposed negative feedback mechanism idea, managed all activities and wrote most of the manuscript. J.S. and J.V. did most of the field and laboratory effort. M.F. did part of the physical modelling and contributed to the preparation and writing of the manuscript. J.Sch. did the frost weathering experiments, studied microstructure and contributed to manuscript preparation. D.M. introduced the soil mechanics perspective, developed the material model and contributed to manuscript writing. A.L.M. and G.K.

contributed to manuscript preparation and writing. J.R. did the triaxial tests and numerical modelling.

Figure captions (not longer than 100 words)

Figure 1. Examples of the selected common sandstone landforms (first column) and their artificial equivalents resulting from partial immersion of Strelec locked sand (SLS) rectangular blocks (second column). The third column presents numerical models showing distribution of the stress indicating the stability of these landforms. Location of the natural landforms is: a, Delicate Arch, Arches National Park, USA; b, Alcove, Navajo Bluff area, USA (photo by V. Cilek); c, Pedestal rock, Angel Arch area, Canyonlands National Park, Utah, USA (photo by V. Cilek); d, Cave pillars, Eladio Cave, Churi Tepui, Venezuela (photo by M. Audy).

Figure 2. Physical modelling with the Strelec locked sand (a-c) and cemented sandstones (d). a, Stable pillar developed from the initial cube sample by decreasing vertical load in steps. b, Relationship between Ssat (horizontal cross-section area of column) and critical vertical stress. c, Relationship between vertical load and tensile strength. d, Comparison of salt weathering rates of unconfined and uniaxially loaded cubes of cemented sandstone. Sample labels are listed in Supplementary Table 3. Photo shows uniaxially loaded sandstone cube converted to a thin pillar by salt weathering.

Figure 3. Continuum mechanics interpretation of the locked sand mechanical behaviour. To describe disintegration of fabric-locked material, we propose so-called “locus of fabric instability”. Locked sand can disintegrate into individual grains by erosion only when the complete stress Mohr circle falls within this locus. σ'_n represents effective normal stress (that

is, total normal stress σ_n minus pore water pressure), τ represents shear stress, φ_p is peak friction angle.

Figure 4. Simplified models of evolution of some basic landforms. Upper row: Cartoon shows onset conditions for four basic types of landform evolution. Bottom row: Cartoon of stabilized landforms: a, Freestanding arch; b, Alcove (lateral cut); c, Pedestal rock; d, Cave pillars (b, c, d - anterior cuts). See Supplementary Figs. 12-17 for more details.


Example from nature
Laboratory experiments
Stress numerical modelling
a Freestanding arch
b Alcove
c Pedestal rock
d Cave pillars
5 cm
5 m
5 cm
5 cm
5 cm
Explanation for numerical modelling:
fabric interlocked material
principal stress direction and magnitude
the maximum level of immersion

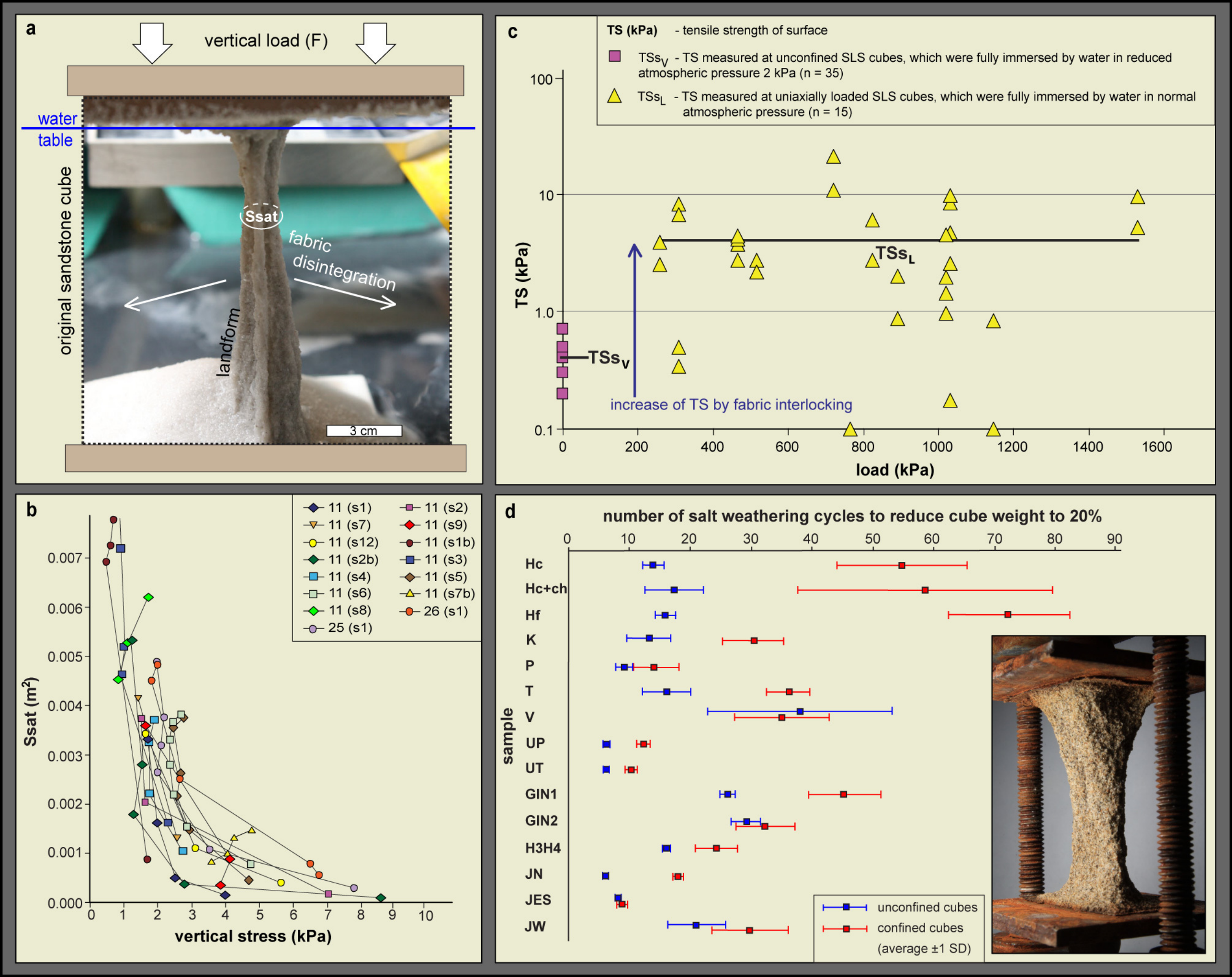
a
vertical load (F)
water table
original sandstone cube
Ssat
fabric disintegration
landform
3 cm
b
Ssat (m²)
vertical stress (kPa)
11 (s1)
11 (s2)
11 (s7)
11 (s9)
11 (s12)
11 (s1b)
11 (s2b)
11 (s3)
11 (s4)
11 (s5)
11 (s6)
11 (s7b)
11 (s8)
26 (s1)
25 (s1)
c
TS (kPa) - tensile strength of surface
TSsV - TS measured at unconfined SLS cubes, which were fully immersed by water in reduced atmospheric pressure 2 kPa (n = 35)
TSsL - TS measured at uniaxially loaded SLS cubes, which were fully immersed by water in normal atmospheric pressure (n = 15)
TS (kPa)
load (kPa)
TSsL
TSsV
increase of TS by fabric interlocking
d
number of salt weathering cycles to reduce cube weight to 20%
sample
Hc
Hc+ch
Hf
K
P
T
V
UP
UT
GIN1
GIN2
H3H4
JN
JES
JW
unconfined cubes
confined cubes
(average ±1 SD)

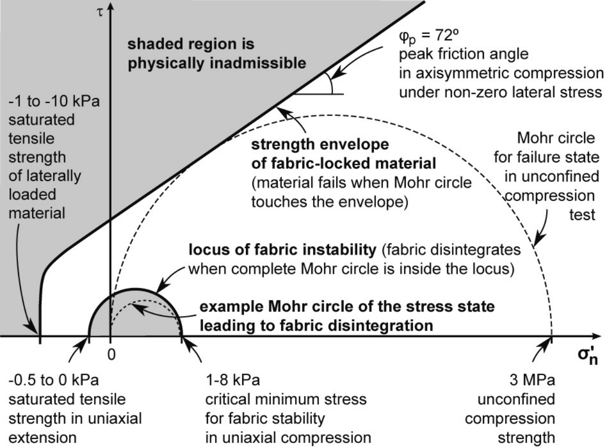
τ
shaded region is physically inadmissible
φ_p = 72º
peak friction angle
in axisymmetric compression
under non-zero lateral stress
-1 to -10 kPa
saturated
tensile
strength
of laterally
loaded
material
strength envelope
of fabric-locked material
(material fails when Mohr circle
touches the envelope)
Mohr circle
for failure state
in unconfined
compression
test
locus of fabric instability (fabric disintegrates
when complete Mohr circle is inside the locus)
example Mohr circle of the stress state
leading to fabric disintegration
0
σ'_n
-0.5 to 0 kPa
saturated tensile
strength in uniaxial
extension
1-8 kPa
critical minimum stress
for fabric stability
in uniaxial compression
3 MPa
unconfined
compression
strength

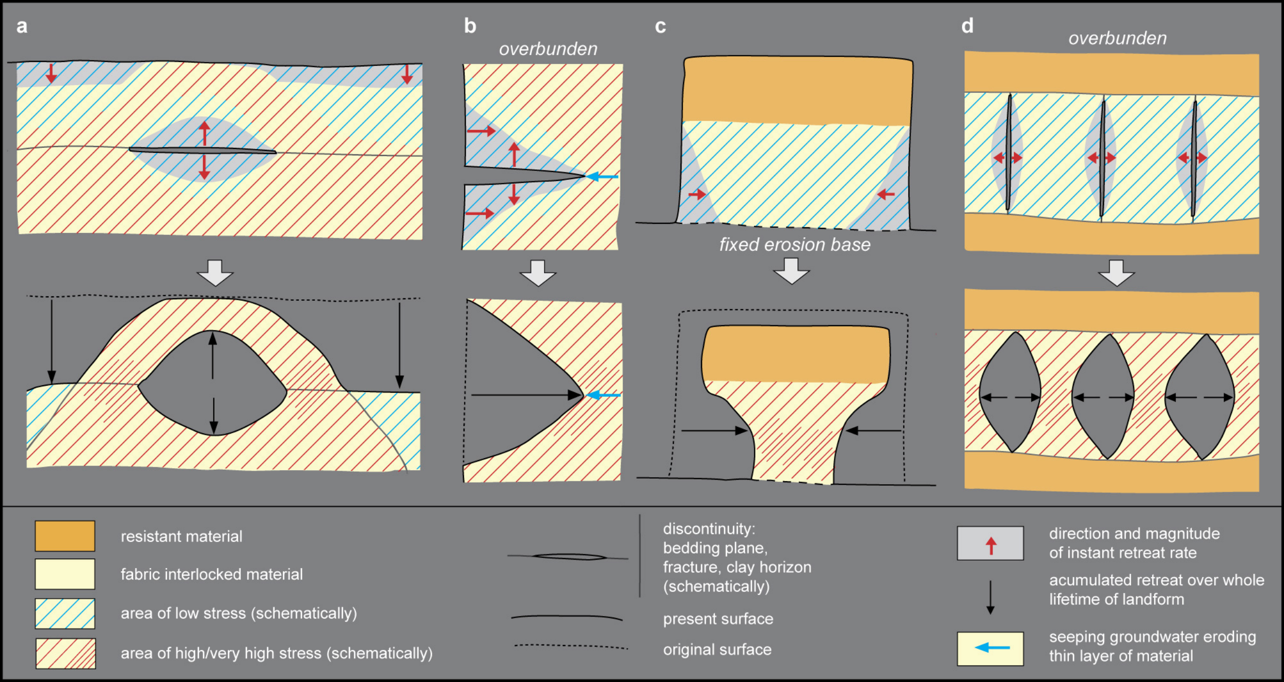
a
b
overbunden
c
d
overbunden
fixed erosion base
resistant material
fabric interlocked material
area of low stress (schematically)
area of high/very high stress (schematically)
discontinuity:
bedding plane,
fracture, clay horizon
(schematically)
present surface
original surface
direction and magnitude
of instant retreat rate
acumulated retreat over whole
lifetime of landform
seeping groundwater eroding
thin layer of material